Journal of Nano- and Electronic Physics
Vol. **11** No 5, 05041(7pp) (2019)

Журнал нано- та електронної фізики
Том **11** № 5, 05041(7cc) (2019)

Effect of Nickel Ions Substitution on the Structural and Electrical Properties of a Nanosized Lithium-iron Ferrite Obtained by the Sol-gel Auto-combustion Method

L.S. Kaykan[1], J.S. Mazurenko[2], I.P. Yaremiy[1], Kh.V. Bandura[2], N.V. Ostapovych[2]

[1] *Vasyl Stefanyk Precarpathian National University, 57, Shevchenko St., 76018 Ivano-Frankivsk, Ukraine*
[2] *Ivano-Frankivsk National Medical University, 2, Halytska St., 76000 Ivano-Frankivsk, Ukraine*

(Received 21 June 2019; revised manuscript received 21 October 2019; published online 25 October 2019)

$Li_{0.5-x/2}Ni_xFe_{2.5-x/2}O_4$ (x = 0.0, 0.2, 0.4, 0.6, 0.8, 1.0) ferrite spinels have been synthesized by sol-gel auto-combustion technique. Structural properties of the obtained powders have been investigated by X-ray diffraction (XRD) method and scanning electron microscopy (SEM). All the synthesized powders have good crystallinity and it is possible to distinguish two spinels of the same composition: the first one of P_4332 spatial group (iron and lithium ions are arranged along ⟨110⟩ crystallographic direction) and the second one of Fd3m spatial group (disordered spinel). The presence of both spinels is observed at low content of the doping material (x = 0.2 and 0.4). In the case of increase in Ni^{2+}, the disordered component is absent and there is only the ordered phase. The particle size values of the synthesized material are calculated using Debye-Scherrer and Williamson-Hall methods. They are of about 22-35 nm. The presence of internal lattice stresses has been detected. According to proposed cation distribution, nickel ions are localized in tetrahedral sublattice and lithium ions are localized in octahedral one. Iron ions are redistributed in both sublattices in the ratio of about 1:2. The Mossbauer spectra represent a superposition of two magneto-ordered components corresponding to the octahedral and tetrahedral surroundings of iron in the spinel lattice and the paramagnetic doublet that indicates the presence of iron in the bivalent state. It is shown that the conductive and dielectric properties of the synthesized powders are characterized by frequency dependence that is characteristic for ferrite materials. The behavior of this dependence is explained on the basis of the hopping mechanism of conductivity and intergranular polarization.

Keywords: Ferrites, Sol-gel auto-combustion, X-ray diffraction, Conductive and dielectric properties.

DOI: 10.21272/jnep.11(5).05041

PACS numbers: 71.20.Nr, 72.15.Eb, 72.20.Pa, 77.22.Gm, 73.22. – f, 76.80. + y

1. INTRODUCTION

Spinel ferrites of the general formula $(Me, Fe)_3O_4$ attract considerable attention due to their excellent physical and chemical properties, as well as an extremely wide range of applications including magnetic storage devices, magnetic leads, telecommunication, microwave devices, gas sensors , magnetic diagnostics, transportation of medicines and much more [1]. Each field of ferrites application requires special properties that can be directly changed selecting the conditions and methods of synthesis as well as the intercalation of certain ions [2]. In particular, for medical and biological applications, such materials should have a magneto-soft behavior at room temperature with low losses at Eddy currents at high frequencies, as well as electrical and optical properties and good chemical and physical stability. Among the various investigated ferrites, nanosized Ni-containing ferrites exhibit small hysteresis, making them a good candidate for use in the medical field [3].

The ferrite spinel crystallizes in the face-centered cubic (fcc) structure of the Fd3m spatial group, in which the unit cell consists of 8 formula units. 32 oxygen ions are located in the nodes of the fcc structure and 24 metal cations are distributed between two types of non-equivalent positions: 64 tetrahedral (A) and 32 octahedral (B) sites, in which metal cations are surrounded by 4 and 6 oxygen ions, respectively [3, 4]. According to the cationic distribution, the spinel structure can be realized in one of three types: normal, inverse and a mixed spinel. Bulk $LiFe_2O_4$ ferrite crystalizes in the inverse spinel structure, in which Li^+ ions occupy B-sites while Fe^{3+} ions are distributed between A and B-sites [5, 6]. However, the cationic distribution depends on a number of factors, one of which is the synthesis process. It was found that nanosized substituted (LiNi)-ferrites could have an inverse spinel structure [7, 8], and also a mixed one – in the case when sizes of Ni ferrite nanoparticles are less than several nanometers [9], that is some Ni^{2+} ions occupy A-sites, displacing an equal number of Fe^{3+} ions to B-sites. The degree of inversion in spinel may vary under different synthesis conditions.

In this paper, we propose the investigation results of the effect of Ni^{2+} ions substitution into the base $Li_{0.5}Fe_{2.5}O_4$ lithium iron spinel obtained by a simple and low cost sol-gel auto-combustion route on its structural and electrical properties.

2. METHODOLOGY

Nickel-substituted $Li_{0.5-x/2}Ni_xFe_{2.5-x/2}O_4$ lithium-iron spinels were synthesized by sol-gel auto-combustion method. $Fe(NO_3)_3{\cdot}9H_2O$ iron, $LiNO_3$ lithium, and $Ni(NO_3)_2{\cdot}6H_2O$ nickel nitrates, citric acid and aqueous ammonia solution were used as precursors. Calculated according to stoichiometry, the starting compounds were dissolved in distilled water and mixed dropwise until a homogeneous solution was obtained. To obtain a pH value of 7, an aqueous solution of ammonia was added dropwise to the resulting precursor solution. The obtained mixture was dried until xerogel formation. The xerogel was placed in the furnace and heated to a temperature of approximately 200-220 °C that caused its flaming. As a result of the exothermic reaction, a

synthesis of ferrite was carried out. The reaction occurred rapidly (about a few minutes) and as a result, a single-phase spinel was obtained as shown by X-ray diffraction analysis.

X-ray diffraction patterns of the synthesized powder systems were obtained using an X-ray diffractometer Ultima-IV, (Rigaku, Japan) in Cu-K_α radiation at room temperature in Bragg-Brentano geometry, in the angle range of 25-90°. The analytical processing of experimental XRD patterns was carried out using the Rietveld method in the *fullproff* software, coherent scattering regions (CSR) sizes were calculated using Selyakov-Scherrer and Williamson-Hall methods.

^{57}Fe absorption spectra were obtained using a MS1104EM Mossbauer spectrometer (^{57}Co source, chromium matrix, activity – 100 mCi. Interpretation of the received spectra was carried out in the Univem package with the calibration relative to α-Fe.

The morphology of the samples surface was studied using a FE-SEM QUANTAFEG 250 scanning electron microscope. The scanning was done at an accelerating voltage value of 15 kV.

Investigation of the conductive and dielectric properties of the samples was carried out using the Autolab PGSTAT 12/FRA-2 impedance spectrometer in the frequency range of 0.01 Hz to 100 kHz.

3. RESULTS AND DISCUSSION

3.1 Structural Analysis and Morphology

XRD patterns of synthesized $Li_{0.5-x/2}Ni_xFe_{2.5-x/2}O_4$ (where x = 0.2, 0.4, 0.6, 0.8, 1.0) spinel system are shown in the Fig. 1.

All samples are crystalline, and one can emphasize two spinels of the same composition: the first one of P_4332 spatial group, the so-called spinel with a superstructure, in which the iron and lithium ions are arranged along the ⟨110⟩ crystallographic direction and the other one of Fd3m spatial group – disordered spinel. The presence of both spinels is observed with low content of the doped element (x = 0.2 and 0.4). In the case of an increase in Ni^{2+}, the disordered component disappears and only the ordered phase remains. In addition to the above phases, systems also have a low content of metallic nickel. Table 1 shows the phase composition of the obtained samples.

Obviously, the presence of metallic nickel can be explained as follows. At the first stage of the auto-combustion reaction, there is a decomposition of precursors and the formation of initial compounds oxides. The remnants of the carbon black frame of citric acid during the burning process reduce part of nickel oxide to the metallic state.

The specified lattice parameters of each component are given in Table 2.

With the increase in Ni^{2+} ions content, the value of the lattice constant of the P_4332 dominant phase increases, which is in agreement with Vegard law.

Table 1 – Phase composition of the synthesized systems

Composition	0.2	0.4	0.6	0.8	1.0
P_4332	63.32	95.22	92.9	92.77	83.76
Fd3m	35.01	2.58	0	0	0
Ni	1.67	2.2	7.1	7.23	16.24

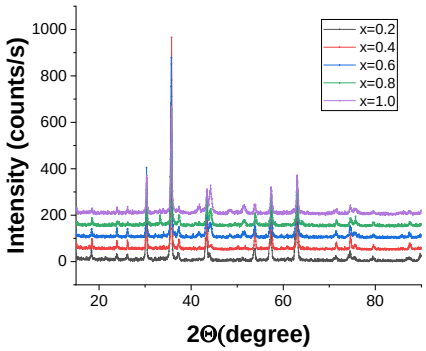

Fig. 1 – XRD patterns of nanocrystalline $Li_{0.5-x/2}Ni_xFe_{2.5-x/2}O_4$ ferrites obtained by sol-gel auto-combustion method

Table 2 – The value of the lattice parameter for each phase of the synthesized samples

Composition	0.2	0.4	0.6	0.8	1.0
P_4332	8.333	8.337	8.339	8.339	8.341
Fd3m	8.376	8.315	0	0	0
Ni	3.550	3.550	3.550	3.550	3.549

The dimensions of the CSR were determined from the full width at half maximum (FWHM) of the lines using the Scherrer formula

$$D = \frac{k\lambda}{\beta\cos\theta}, \qquad (1)$$

where λ is the X-ray wavelength (1.54056 Å), θ is the diffraction angle, β is the full width at half maximum and k is the Scherrer constant (k = 0.94 for particles close to spherical cubic symmetry) [21]. However, the dependence of cosθ on 1/β (Scherrer's dependence) is not approximated by line well (see the insertion in Fig. 2). Williamson-Hall equation is more precise. It binds both the crystallite size and the strain in the lattice, which are caused by the peak broadening:

$$\beta = \beta_{size} + \beta_{strain} = \frac{k\lambda}{D\cos\theta} + 4\varepsilon\tan\theta, \qquad (2)$$

where ε is the microstrain parameter, and other symbols have the above meanings. Dependence of $\beta\cos\theta$ on $4\sin\theta$ is shown in Fig. 2 (W-H dependence).

This dependence is a set of points with a small scatter that indicates the uniformity of lattice strains and, thus, isotropic nature of samples. Moreover, the dependence shows a positive inclination/slope, which is the evidence of the presence of elastic strains in the nanoparticles. The crystallite (grain) sizes and the microstrain values of the samples that are determined according to the intersection and inclination/slope of the W-H dependence are shown in Table 3. As can be seen from Table 3, there is no apparent tendency of influence of the substituting element content on the crystallite sizes. Somewhat higher values of CSR for samples x = 0.0 (42 nm) and x = 0.4 (35 nm) are obviously related to the auto-combustion reaction rate, which depends on the metal/fuel ratio [10].

The morphology of the synthesized samples was investigated using scanning electron microscopy (SEM). SEM images of the obtained systems and their chemical composition are shown in Fig. 3. As can be seen from

SEM images, the particles are agglomerates consisting of smaller particles with close to spherical shape.

Taking into account the spherical form of the synthesized particles, their active surface area (SSA, total surface area per unit mass) can be calculated as

$$S = \frac{A}{\rho D'}, \qquad (3)$$

where A is a shape factor, for spherical particles $A = 6$ [25], D' is the particle size and ρ is the sample density. The theoretical (X-ray) density of our cubic compounds was calculated according to the formula [26]:

$$\rho_x = \frac{ZM}{N_A a^3}, \qquad (4)$$

where Z is the number of formula unit per unit cell (in this case $Z = 8$), M is a molecular mass of the compound and N_A is Avogadro's number. Calculated density and the specific surface area values are shown in Table 3.

Ions of substituted nickel are localized in the tetrahedral sublattice, whereas lithium and about 2/3 of iron ions are in the octahedral sublattice. Cation distribution under sublattice with increasing substitution obtained by Rietveld method is shown in Table 4.

In the papers [9, 11, 12] on the study of $NiFeO_4$ nanoparticle composition, the following distribution was proposed: $\left(Ni_{1-i}^{2+}Fe_i^{3+}\right)_A\left(Ni_i^{2+}Fe_{2-i}^{3+}\right)_B O_4$. Since the lithium ions have the greatest ionic radius, it is logical to assume that it will be localized in the octahedral sublattice. Since, according to the X-ray diffraction analysis, it is impossible to directly determine the localization of lithium ions due to the small number of electrons, this distribution was proposed according to experimental data on the distribution of iron and nickel ions and logical assumptions. These works [10-12] confirm our results on the octahedral localization of lithium ions.

Based on experimentally obtained values of the lattice constant and oxygen parameter (u), the ionic radii values were calculated for the tetrahedral r_A and octahedral r_B positions using formulas [13]:

$$r_A = C_{ANi} r\left(Ni^{2+}\right) + C_{AFe} r\left(Fe^{3+}\right), \qquad (5)$$

$$r_B = \frac{1}{2}\left[C_{BFe} r\left(Fe^{3+}\right) + C_{BLi} r\left(Li^{+}\right)\right], \qquad (6)$$

where $r(Li^+)$, $r(Ni^{2+})$, $r(Fe^{3+})$ are the ionic radii, which have the following values

$$r_A(Ni^{2+}) = 0.55 \text{ Å}, \; r_B(Li^+) = 0.72 \text{ Å},$$

$$r_A(Fe^{3+}) = 0.49 \text{ Å}, \; r_B(Fe^{3+}) = 0.645 \text{ Å},$$

and C_{ANi}, C_{AFe}, C_{BFe}, C_{BLi} are the concentrations of the corresponding ions in the A and B-sublattices. Calculated values of ionic radii for each composition and each sublattice are given in Table 5.

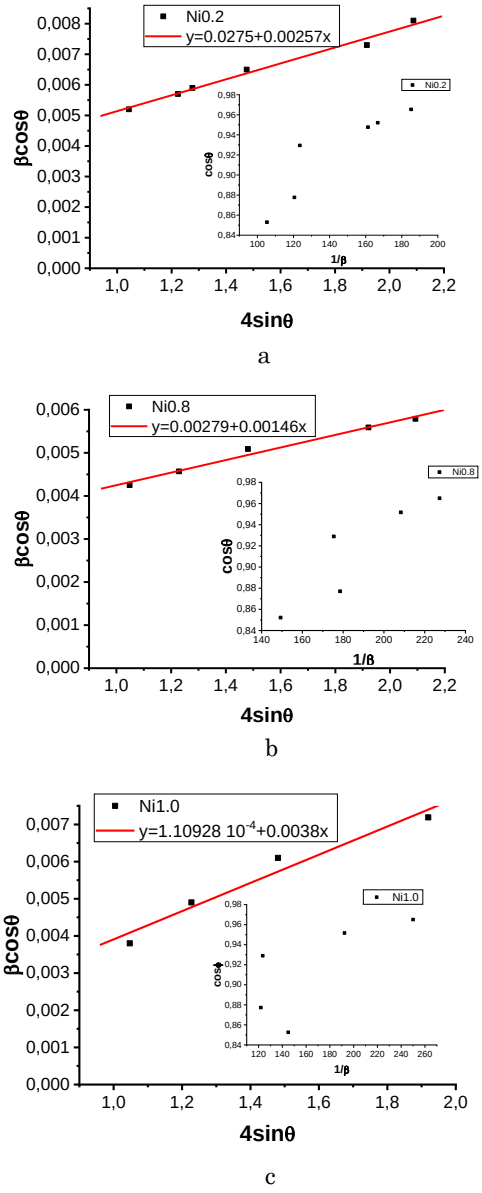

Fig. 2 – Williamson-Hall (left) and Debye-Scherrer (right) dependences for $Li_{0.5-x/2}Ni_xFe_{2.5-x/2}O_4$ nanoparticles with different nickel contents

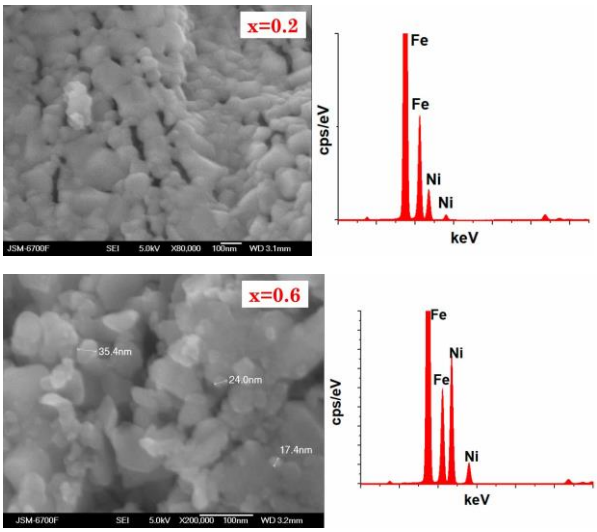

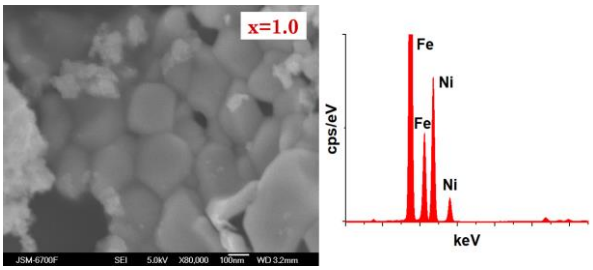

Fig. 3 – SEM images of the obtained systems and their chemical compositions

As can be seen from Table 5, when the content of nickel increases, the size of tetrahedral holes gradually increases and of octahedral ones decreases. This is due to an increase in nickel in tetrahedral sublattice and a decrease in lithium with a large ionic radius in octahedral sublattice. Some deviations from monotonicity are obviously caused by the presence of a phase of metallic lithium, the content of which increases from 1.7 ($x = 0.2$) to 7.23 ($x = 0.8$).

Table 3 – The crystallite (grain) sizes and the microstrain values of the samples that are determined according to the intersection and inclination of the W-H dependence

Composition	Molar mass M	Hopping length d_A, nm	Hopping length d_B, nm	Crystallite sizes D, nm	Value of microstrain ε	X-ray density ρ, g/cm^3	Specific surface area S, (10^6 cm^2/g)
$x = 0.0$	207.095	0.3607	0.2945	42.1	0.0045	4.77	0.299
$x = 0.2$	212.5544	0.3608	0.2946	22.96	0.0026	4.89	0.534
$x = 0.4$	218.0133	0.3610	0.2947	34.86	0.0016	5.21	0.330
$x = 0.6$	223.4722	0.3611	0.2948	29.75	0.0012	5.25	0.394
$x = 0.8$	228.9311	0.3611	0.2948	29.02	0.0014	3.95	0.523
$x = 1.0$	234,39	0.3643	0.2974	26.71	0.0038	3.04	0.242

Table 4 – Cation distribution

x	A-site	B-site	a, nm	Δa, nm
0.0	$Fe_{1.0}$	$Li_{0.5}Fe_{1.41}$	0.8330	± 0.0002
0.2	$Ni_{0.2}Fe_{0.78}$	$Li_{0.4}Fe_{1.62}$	0.8333	± 0.0002
0.4	$Ni_{0.4}Fe_{0.66}$	$Li_{0.3}Fe_{1.54}$	0.8337	± 0.0002
0.6	$Ni_{0.56}Fe_{0.43}$	$Li_{0.2}Fe_{1.47}$	0.8339	± 0.0002
0.8	$Ni_{0.74}Fe_{0.21}$	$Li_{0.1}Fe_{1.39}$	0.8339	± 0.0002
1.0	$Ni_{0.93}Fe_{0.11}$	$Fe_{1.34}$	0.8412	± 0.0002

Table 5 – Average ionic radii at A and B sites ($\langle r_A \rangle$ and $\langle r_B \rangle$, respectively), oxygen positional parameter (u) and site occupancy in $Li_{0.5-x/2}Ni_xFe_{2.5-x/2}O_4$ nanoparticles synthesized at different pH values of 9 and 11

Concentration, x	a_{exp}, (Å)	a_{th}, (Å)	r_A, (Å)	r_B, (Å)	$\bar{r}$, (Å)	u, (Å)
0.0	8.330	8.208	0.490	0.635	0.562	0.3721
0.2	8.333	8.295	0.490	0.667	0.578	0.3760
0.4	8.337	8.305	0.543	0.605	0.574	0.3778
0.6	8.339	8.316	0.519	0.527	0.523	0.3759
0.8	8.339	8.327	0.510	0.484	0.497	0.3759
1.0	8.412	8.319	0.565	0.432	0.524	0.3715

Fig. 4 shows the diffractograms of the synthesized samples that are interpreted using the *fullproff* program.

3.2 Mössbauer Studies

In order to clarify the cation distribution and to establish the nature of the magnetic ordering of the synthesized systems, Mössbauer studies at room temperature were carried out. Mössbauer spectra ^{57}Fe of investigated systems are shown in Fig. 5.

The obtained spectrum is a superposition of two sextets that corresponds to tetrahedral and octahedral positions of iron atoms in the spinel sublattices. The values of the magnetic field strength are 507 and 492 kOe, respectively. In addition, the paramagnetic doublet with a quadrupole splitting of ~ 2.5 mm/s is observed in the Mössbauer spectrum. The appearance of this doublet is explained by the presence of iron with the valence of 2. The value of the isomer shift in all the investigated systems is of about 0.2-0.4 mm/s that is the evidence of the iron presence in Fe^{3+} state with $3d^5 4s^0$ electronic configuration.

The value of quadrupole splitting for all systems is very small (close to zero) that indicates that the field around the nucleus is spherically symmetric and there are no significant deviations from spherical symmetry.

Sufficiently large values of the linewidth (0.46 mm/s) indicate that the samples are fine crystalline and their size distribution is practically continuous.

3.3 Conductive and Dielectric Properties

Conductive and dielectric properties of synthesized nanosized samples of $Li_{0.5-x/2}Ni_xFe_{2.5-x/2}O_4$ composition were investigated at room temperature in a wide frequency range using an impedance spectrometer.

Fig. 6 shows a change of the real and imaginary parts of the dielectric permeability with frequency. Both the real and imaginary parts decrease with increasing frequency and are almost constant at a frequency of ≥ 100 Hz.

This behavior of dielectric permeability is a consequence of the fact that electric dipoles, beginning with a certain frequency, do not have time to reorient in the

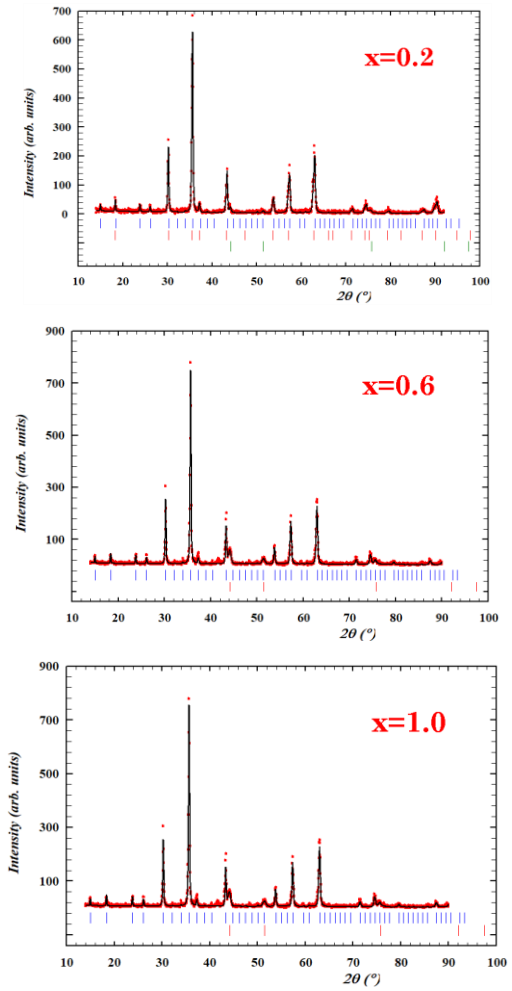

Fig. 4 – XRD diffractograms of the synthesized samples that are decoded using the *fullproff* program

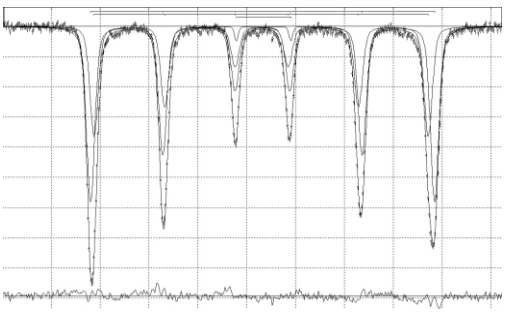

Fig. 5 – Mössbauer spectrum ^{57}Fe of the $Li_{0.4}Fe_{2.4}Ni_{0.4}O_4$ system obtained at room temperature

direction of the external field when increasing its frequency. The high value of the dielectric constant in the low-frequency region is the result of spatial polarization that occurs at the boundaries of the grains, which create a potential barrier. As a result, there is a charge accumulation on the grain boundaries that leads to a high value of the dielectric constant at low frequencies [14]. The behavior of the real part of the dielectric permeability also depends on the existence of a significant number of trapping centers between the valence band and the conduction band [15]. These trapping states arise as a result of the defect formation, in particular the Frenkel and Schottky types during the crystallization process of samples when synthesized by sol-gel auto-combustion. Polarization in spinel ferrites is associated with the charge carrier hops, and thus, the accumulation of charges on interphase and intergrain boundaries occurs at low frequencies. This is due to their high resistance and this is the cause of high values of the dielectric constant.

With an increase in the frequency of the external electric field, the frequency of electric dipoles reorientation lags behind the change in the direction of the external electric field and thus dielectric permeability decreases. The non-monotonic behavior of the dielectric permeability, which depends on the nickel ions content, is the result of changes in the cationic distribution of Fe^{3+} and Ni^{2+} ions in octahedral and tetrahedral sites as well as the microstructure of the specimens, which is sensitive to the method and conditions of synthesis. The dependences of the real and imaginary parts of specific electrical conductivity of samples on the frequency are given in Fig. 7.

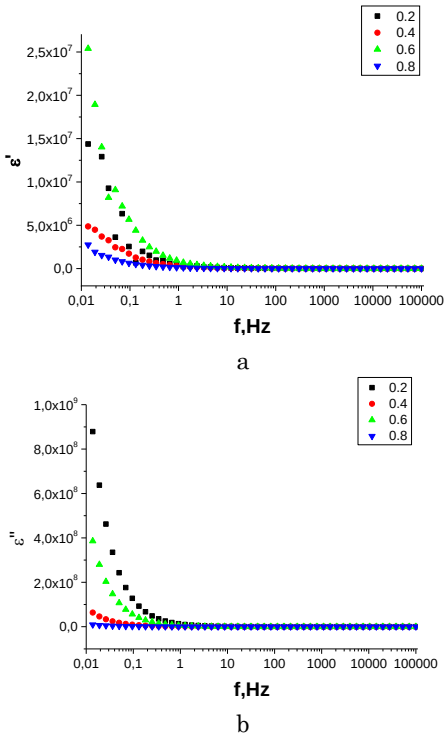

Fig. 6 – Change of the real (a) and imaginary (b) parts of the dielectric permeability with frequency at different nickel ion contents

In spinel ferrite materials, an electrical conductivity is an attribute of the hop of an electron between ions with variable valence. In the case of Ni^{2+} substitution, the hopping conductivity can be realized by two ways:

$$Fe^{3+} + e^- \leftrightarrow Fe^{2+} \text{ and } Ni^{3+} + e^- \leftrightarrow Ni^{2+}.$$

It can be seen from Fig. 7 that the electrical conductivity does not depend on the frequency at low frequencies that corresponds to the *DC* conductivity and it is related to the grain boundaries, which are more effective at low frequencies and have high resistance value. In addition, it can be noted that the electrical conductivity depends on the frequency at high frequencies, and this area can be attributed to the *AC* conductivity.

For all samples obtained by sol-gel auto-combustion method, *AC* conductivity increases with increasing frequency.

This is due to the fact that the electric energy associated with the applied alternating field contributes to the oscillations of the trapped charges and their transfer between different localized states [16]. Moreover, an increase in conductivity with a further increase in frequency is associated with the magnitude of the hop between ions of different valency in the investigated spinel ferrites.

The dependence of the real part of the dielectric permeability and specific resistance on the content of Ni^{2+} ions is shown in Fig. 8.

As can be seen from Fig. 8, these values are sensitive to the nickel content. Thus, the dielectric and conductive properties of obtained nanosized ferrite spinels can be optimized by substitution.

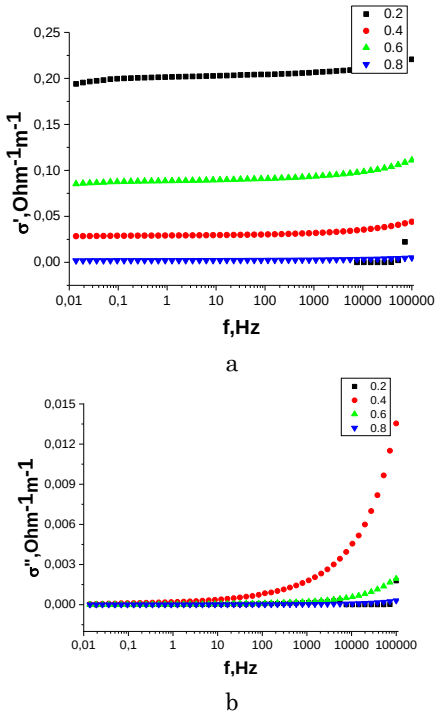

Fig. 7 – Frequency dependence of the real (a) and imaginary (b) parts of the electrical conductivity of $Li_{0.5-x/2}Ni_xFe_{2.5-x/2}O_4$ systems obtained by sol-gel auto-combustion method

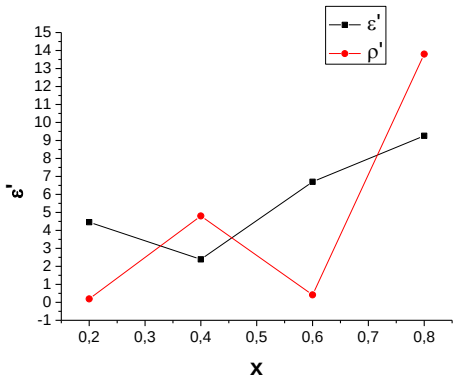

Fig. 8 – The dependence of the real parts of the dielectric permeability and the specific resistance on the Ni^{2+} ions content

4. CONCLUSIONS

Nanosized spinel ferrites of the $Li_{0.5-x/2}Ni_xFe_{2.5-x/2}O_4$ composition, where $x = 0.0$, 0.2, 0.4, 0.6, 0.8, 1.0, have been obtained by sol-gel auto-combustion method. At low substitution doses, two spinels of the same composition coexist in the structure: the first one of P_4332 spatial group, the so-called spinel with superstructure, in which the iron and lithium ions are ordered arranged along the ⟨110⟩ crystallographic direction, and the other one of Fd3m spatial group – disordered spinel. The presence of both spinels is observed at the low content of the doped element ($x = 0.2$ and 0.4). In the case of an increase in Ni^{2+} ions, the disordered component disappears and only the ordered phase remains. In addition to the above phases, the systems also have a low content of metallic nickel. Particle sizes of the synthesized product are 22-35 nm. According to the proposed cation distribution, nickel ions are localized in the tetrahedral sublattice and lithium ions – in the octahedral one. Iron ions are redistributed in both sublattices according to the ratio of approximately 1:2. It is shown that the conductive and dielectric properties of synthesized powders are characterized by frequency dependence characteristic of ferrite materials, the behavior of which is explained on the basis of the hopping conductivity mechanism and intergrain polarization. These characteristics are sensitive to nickel content, peculiarities of cation distribution and microstructure.

REFERENCES

1. M. Zamani, E. Naderi, M. Aghajanzadeh, *J. Mol. Liquid.* **274**, 60 (2018).
2. A.G. Abraham, A. Manikandan, E. Manikandan *J. Magn. Magn. Mater.* **452**, 380 (2018).
3. G. Wang, F. Zhou, X. Li, *Ceram. Int.* **44**, 13588 (2018).
4. R. Singh Yadav, I. Kuřitka, J. Havlica, *J. Magn. Magn. Mater.* **208**, 13 (2000).
5. A.G. Hufnagel, K. Peters, A. Müller, *Adv. Funct. Mater.* **26**, 4435 (2016).
6. M.V.-Vasic, E.S. Bozin, L. Bessais, *J. Phys. Chem. C* **117**, 12358 (2013).
7. H.F. Abosheiasha, S.T. Assar, *J. Magn. Magn. Mater.* **370**, 54 (2014).
8. A. Ghasemi, M. Mousavinia, *Ceram. Int.* **40**, 2825 (2014).
9. P. Iranmanesh, Sh. Tabatabai Yazdi, M. Mehran, S. Saeednia, *J. Magn. Magn. Mater.* **449**, 172 (2017).
10. A.K. Sijo *J. Magn. Magn. Mater.* **441**, 672 (2017).
11. Charalampos Stergiou, *J. Magn. Magn. Mater.* **426**, 629 (2017).
12. K.S. Aneesh Kumar, R.N. Bhowmik. *Mater. Chem. Phys.* **146**, 159 (2014).
13. B.K. Ostafiychuk, L.S. Kaykan, J.S. Kaykan, *Nanoscale. Res. Lett.* **12**, 237 (2017).
14. M.A. Dar, D. Varshney *J. Magn. Magn. Mater.* **436**, 101 (2017).
15. H.M. Tahir Farid, I. Ahmad. *J. Magn. Magn. Mater.* **434**, 143 (2017).
16. K. Jalaiah, K. Vijaya Babu, *J. Magn. Magn. Mater.* **423**, 275 (2017).

Вплив заміщення іонів нікелю на структуру і електричні властивості нанорозмірного літій-залізного фериту, отриманого методом золь-гель автогоріння

Л.С. Кайкан[1], Ю.С. Мазуренко[2], І.П. Яремій[1], Х.В. Бандура[2], Н.В. Остапович[2]

[1] *ДВНЗ "Прикарпатський національний університет імені Василя Стефаника", вул. Шевченка, 57, 76018 Івано-Франківськ, Україна*
[2] *Івано-Франківський національний медичний університет, вул. Галицька, 2, 76000 Івано-Франківськ, Україна*

Методом золь-гель автогоріння були синтезовані ферити шпінелі складу $Li_{0.5-x/2}Ni_xFe_{2.5-x/2}O_4$ (де $x = 0.0, 0.2, 0.4, 0.6, 0.8, 1.0$). Структурні властивості отриманих порошків досліджувалися за допомогою рентгенівської дифракції (XRD), мессбауерівської спектроскопії, а також з використанням скануючої електронної мікроскопії (SEM). Усі синтезовані зразки володіють гарною кристалічністю, причому можна виділити дві шпінелі однакового складу: одна просторової групи P_4332, в якій іони заліза і літію упорядковано розміщені вздовж кристалографічного напрямку ⟨110⟩, а інша – просторової групи Fd3m, розупорядкована шпінель. Присутність обох шпінелей спостерігається при низькому вмісті допійованого елементу ($x = 0.2$ і 0.4). У випадку збільшення Ni^{2+} розупорядкована компонента зникає і залишається тільки упорядкована фаза. Розміри частинок синтезованого продукту, отриманих методами Дебая-Шеррера і Вільямсона Холла, складають 22-35 нм. Виявлена присутність внутрішніх напруг гратки. Згідно запропонованого катіонного розподілу іони нікелю локалізуються у тетрапідгратці, а іони літію – у октапідгратці. Іони заліза перерозподіляються по обох підгратках у співвідношенні приблизно 1:2. Мессбауерівські спектри являють собою суперпозицію двох магнітоупорядкованих компонент, що відповідають октаедричному і тетраедричному оточенню заліза в шпінельній гратці і парамагнітного дублету, який вказує на присутність заліза у двовалентному стані. Показано, що провідні і діелектричні властивості синтезованих порошків мають характерну для феритових матеріалів частотну залежність, поведінка якої пояснюється на основі стрибкового механізму провідності і міжзеренної поляризації.

Ключові слова: Ферити, Золь-гель автогоріння, Рентгенівська дифракція, Провідні і діелектричні властивості.